University of Birmingham

Flexural behaviour of concrete thin sheets prestressed with basalt-textile reinforcement

Hutaibat, Mohammed; Ghiassi, Bahman; Tizani, Walid

[Link to publication on Research at Birmingham portal](#)

Flexural behaviour of concrete thin sheets prestressed with basalt-textile reinforcement

Mohammed Hutaibat [a], Bahman Ghiassi [b,*], Walid Tizani [a]

[a] Centre for Structural Engineering and Informatics, Faculty of Engineering, University of Nottingham, Nottingham NG7 2RD, United Kingdom
[b] School of Engineering, University of Birmingham, Birmingham B15 2TT, United Kingdom

ARTICLE INFO

ABSTRACT

While the recently emerged textile-reinforced concrete (TRC) composites offer a more durable alternative to conventional reinforced concrete, these composites are susceptible to cracking and high deformations under service loads, which hinders their widespread application for the development of load-bearing structural components. Aiming at addressing this issue, the present paper experimentally investigates the flexural response of non-prestressed and prestressed basalt-based textile-reinforced concrete plates. Basalt is chosen as an emerging low-carbon reinforcement for TRC composites. The first series of tests is focused on non-prestressed TRCs and consists of eleven reinforcement configurations considering the role of reinforcement ratio, position and coating on the flexural behaviour of TRCs. The second series, focused on prestressed TRCs, considered the role of pre-stressing level (13%, 25% and 35% of the fabric's ultimate tensile load), releasing time, testing age and coating type on the flexural behaviour.

1. Introduction

Textile-reinforced concrete (TRC) combines non-metallic mesh-like fabrics and a fine-grained concrete matrix [1,2] to form a high-performance composite material that provides a competitive and more durable alternative to conventional reinforced concrete [3,4]. Given its significant mechanical properties and pseudo-ductile response, TRC is well-suited for the retrofitting and seismic strengthening of masonry and concrete structures [5–8]. The application of TRCs to the manufacturing of new concrete components also allows the production of lighter and thinner structural members because of their high strength-to-weight ratio [9].

Although a growing number of investigations have been devoted to a better understanding of the mechanical performance of TRC composites, the focus has been mostly on the load-bearing capacity of TRC components under flexural or tensile loads [10–12]. Even though there is still a lack of comprehensive understanding of the structural behaviour of components made of these composites [13]. The role of production tolerance, reinforcement ratio, or reinforcement position on the mechanical response of TRCs has yet to be fully investigated [4,14]. The existing data have shown the susceptibility of TRCs to cracking and high deformations under service loads [15], which can hinder their

widespread application to load-bearing structural components. Addressing this challenge calls for a range of potential solutions, including surface modification techniques (i.e. impregnation and coating) [16–20], incorporation of short fibres [21,22], and the application of prestressing to the textile reinforcement [23–26]. While prestressing holds promise as a solution, it has only received little and scarce attention to date. Prestressing concrete structures improves mechanical strength, structural performance, bonding, and rigidity [23,24]. This approach effectively utilises the material's high tensile strength, minimising excessive deflections from passive reinforcement's low stiffness [25]. Moreover, it reduces cracks due to shrinkage and loads, creating durable, crack-free slender elements.

For the application of prestressing technology to TRCs, the development of appropriate test setups that ensure uniform prestressing of the yarns remains a challenge. Selection of a suitable textile (high tensile strength, high elastic modulus and, low relaxation) and matrix (sufficient workability, high initial and final strength, and low shrinkage) are vital to a successful prestressing application. The bond between textile reinforcement and the concrete matrix and that in between the filaments also plays a significant role in the efficiency of prestressing technique in TRC composites. Coating and impregnation of the textiles generally help in improving the interfilament and textile-to-concrete bond

---

* Corresponding author.
E-mail addresses: mohammed.hutaibat@nottingham.ac.uk (M. Hutaibat), b.ghiassi@bham.ac.uk (B. Ghiassi), walid.tizani@nottingham.ac.uk (W. Tizani).

performance, helping in better efficiency of prestressing applications [27,28]. Non-impregnated textiles generally perform worse under prestressing loads, which is also dependent on the type of fibres (e.g. prestressed TRCs made of non-coated dry carbon fibres, despite having higher tensile strength and elastic modulus than non-coated dry AR glass fibres, showed a poorer performance due to their weaker bond with cementitious matrix and reduction of the interfilament friction after prestressing) [27,28].

As such, carbon, basalt, or aramid reinforcements are considered to be more propitious for prestressing applications [26–31]. Although notable prestress losses were observed in prestressed aramid-based TRCs due to the considerable relaxation of aramid fibres when exposed to alkaline environments (commonly present in a cementitious matrix) and the interfilament bond deterioration following the introduction of prestressing forces [31,32]. On the other hand, the susceptibility of AR-Glass fibres to alkaline degradation and poor creep resistance due to stress corrosion or static fatigue makes them unsuitable for prestressing applications [33,34]. Therefore, the utilisation of materials with specific physical attributes is crucial for achieving functional prestressed composites of desired strength and stiffness. Materials like basalt fibres have demonstrated their chemical robustness and favourable physical properties within sectors such as the aerospace and automotive industries [35]. The versatile forms of basalt fibres, including ropes, short fibres, bars, and continuous textiles, have emerged as pioneering materials for structural applications [8]. Recently, basalt-based textiles have gained interest as a natural-based, non-toxic, cost-effective, and thermally stable reinforcement for the development of TRCs [36–38]. As such, the existing data on the mechanical performance of non-prestressed and prestressed basalt-based TRCs is scarce [30].

In a recent study, Du et al. [30] investigated the effect of the number of textile layers and prestressing level (i.e. up to 30%) on the flexural properties of coated basalt textiles. They observed that prestressing increased the cracking stress by 50% with a slight improvement in the pre-cracking stiffness, but negatively affected the ultimate bearing capacity and toughness at all prestress levels when compared to non-prestressed counterpart samples. However, further investigations are still needed to understand the performance of basalt textiles in prestressing applications. Textile reinforcement, unlike traditional concrete, is not restricted by concrete cover due to corrosion resistance. It's crucial to explore the performance of TRC components with minimal or no concrete cover, and their potential as external reinforcement to enhance overall composite structure performance. The role of several parameters, such as reinforcement ratio, location of reinforcement, prestressing release time, or testing age on the performance of basalt-based TRCs remains not understood.

Aiming at addressing these gaps, this paper presents a comprehensive experimental campaign on the flexural behaviour of non-prestressed and prestressed Basalt TRCs. For the non-prestressed TRCs, the focus was on understanding the role of reinforcement ratio (0.37%, 0.56%, and 0.93%), reinforcement position, the distance between reinforcement layers (internal lever arm) and textile surface modification using sand coating on the flexural response of TRC plates. For the prestressed TRCs, the role of prestress release time (1-day and 7-day), testing age (7, 28, and 90 days), surface modification (sand coating), and prestressing level (0%, 13%, 25%, and 35%) on the flexural behaviour are investigated and reported.

2. Experimental programme

2.1. Concrete

A single concrete mix was specifically tailored and adopted in this work. The matrix's composition and the hardened concrete's mechanical properties are given in Table 1. The matrix consisted of cement, fly ash, silica fume, and fine aggregate (0.6–1.2 mm). Rapid hardening Portland cement (CEM I) was used to attain the required strength and

Table 1
Mix proportions and mechanical properties of the cementitious binder.

Materials/Properties	Characteristic parameters
Cement (52.5 R)* [Kg/m^3]	589.2
Fly Ash [Kg/m^3]	189.0
Silica Fume [Kg/m^3]	50.3
Sand 0.6–1.0 [Kg/m^3]	1121.6
Water [Kg/m^3]	259.2
Superplasticiser dosage [% weight of total binder]	0.016
Water/binder ratio	0.31
Aggregate/Binder ratio	1.35
Slump [mm]	280
1-day compressive strength** [MPa]	29 (5.7)
7-day compressive strength** [MPa]	65 (6.9)
28-day compressive strength** [MPa]	113 (5.1)
90-day compressive strength** [MPa]	116 (6.3)

* CEMI Rapid hardening concrete. **Compressive strength of concrete is based on samples cured under water. The result's coefficient of variation is presented in parentheses.

bond performance under 24 h [39,40], for resisting prestressing loads once the yarns are released [41]. A polycarboxylate superplasticizer that fulfils the standard requirements in BS EN 197-1:2011 [42] was added to achieve sufficient workability.

The compressive strength of the concrete mix was experimentally determined at different ages (24 hrs, 7, 28, and 90 days) according to ASTM C109 [43]. For this purpose, three identical cubes of 50 mm size were prepared and tested at target ages using a 200 kN servo-controlled universal testing machine at a load rate of 1.5 kN/s. The flowability of the concrete mix was determined using the mini-slump cone method for fine concrete by pouring the concrete in a truncated cone with dimensions shown in Fig. 1 set over a smooth, non-absorbent plate. Once the cone is lifted, the average spread can be calculated over two measurements (D1, D2) [44]. The test results showed the developed mix had a slump of 280 mm and an average compressive strength of 29 MPa at 24 hrs (65 MPa, 113 MPa and 116 MPa at 7, 28, and 90 days, respectively) taken from 3 tested samples.

2.2. Fabric

A flexible, unidirectional basalt textile coated with an alkaline resistance polymer coating was used in this study. The wrap and weft yarns form an open mesh of 25 mm in orthogonal directions (Table 2). The mechanical properties of the textile were characterised by conducting uniaxial tensile tests on at least four identical samples of non-standard bare textile coupons. Textile coupons consisted of two groups of single-yarn and two-yarn coupons. The tested samples had a clear length of 260 mm out of 410 mm total length, with a nominal width of 25 mm and 50 mm for the single and two-yarn coupons, respectively. Strain-compatible steel tabs were glued to both ends of each coupon with epoxy resin to ensure a homogeneous, constant pressure and sufficient grip. The samples were clamped at both ends and tested using an Instron machine under a constant displacement rate of 0.005 mm/sec. During the tests, the applied monotonic load was recorded using the machine's internal load cell, and the specimens' extension was measured using a video gauge over a 200 mm gauge length targeted at the centre of the samples. The key results are listed in Table 2. The ultimate stress (σ_{fu}) of the textile was calculated as follows, from the obtained experimental data:

$$\sigma_{fu} = \frac{f_{fu}}{A_f} \tag{1}$$

$$A_f = b_f * t_f \tag{2}$$

Where f_{fu} is the ultimate tensile load, A_f is the cross-sectional area, b_f is the nominal width of the coupon, and t_f is the nominal thickness of the textile coupon provided by the manufacturer datasheet. The modulus of
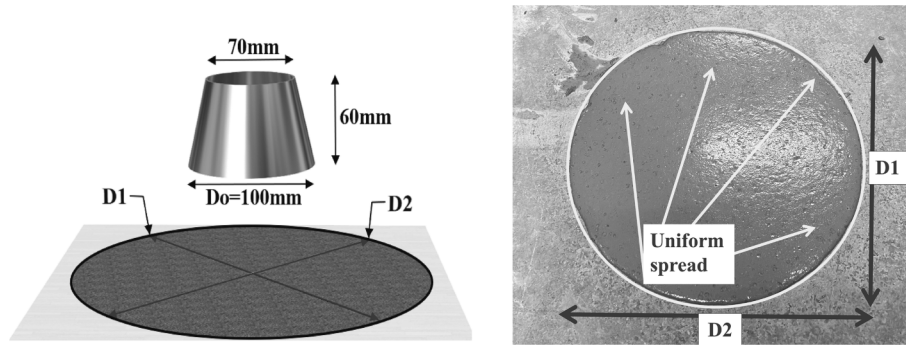
Fig. 1. Mini-slump test schematic view.

Table 2
Mechanical properties of basalt textile.

Properties		Unit	Manufactures' Data	Experimental Data
Mesh size		[mm]	25x25	25x25
Fibre orientation		-	Unidirectional	Unidirectional
E_f[a]		[GPa]	89	81
Weight		[g/m²]	220	-
Density		[g/cm³]	2.67	-
Nominal thickness		[mm]	0.037	-
σ_{fu}[b]	One-Yarn	[MPa]	-	1538 (5.3)
	Two-Yarn	[MPa]	–	1356 (4.0)

*The coefficient of variation is presented in parentheses. [a] E_f: modulus of elasticity. [b] σ_{fu}: ultimate tensile stress.

elasticity (E_f) was found as the slope of the linear part of the curve. Fig. 2 shows the stress–strain curves of the tested coupons. It can be observed that the load increases linearly up to the ultimate load in single-yarn coupons. The results from two-yarn coupons are also consistent with single-yarn results, with the exception of one sample that shows a discrepancy near the ultimate load, which can be attributed to the non-uniform distribution of the stress between yarns and local failure of the filaments.
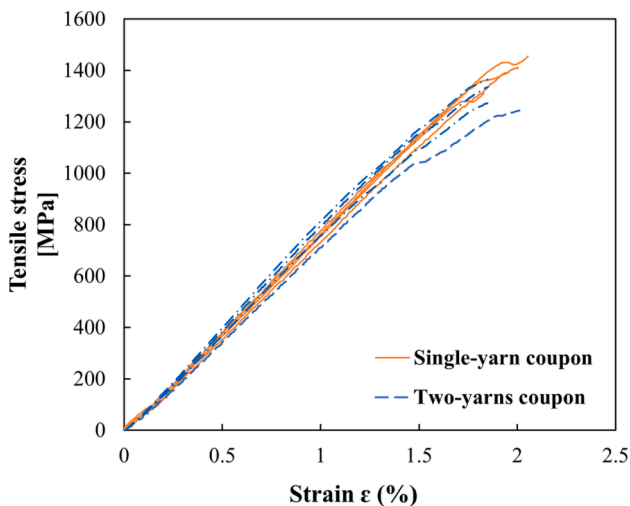

Fig. 2. Tensile stress–strain results on textile coupons (single and two-yarn coupons).

2.3. Test specimens and investigated parameters

The experimental programme was conducted in two stages: the first stage comprised 13 variables (with five identical samples for each configuration) carried out on thin flat non-prestressed TRC plates to investigate the influence of the textile reinforcement configuration (i.e. reinforcement ratio (ρ) and the textile layer (lever arm) position) on the overall flexural performance. The outcomes of this series were used to design the second stage of the tests which was aimed at understanding the flexural performance of prestressed TRC (PTRC) plates. Three different reinforcement ratios (ρ) were combined with different reinforcement locations, leading to a total of 11 configurations. The reinforcement ratio was calculated by dividing the textile's total cross-sectional area ($A_{f = t_f} *b$) by the plate cross-sectional area ($b*h$), where t_f is the equivalent thickness of the textile, b and h are the width and thickness of the plate, respectively. Hereafter, the reinforcement configuration will be indicated by the letter (C) in the specimen's nomenclature (see Fig. 3). Two, three, and five plies of textile reinforcement were embedded in the matrix with different configurations, presented by measuring the bending depth (d_x) of the textile layer with respect to the top of each sample (Fig. 3). This led to the establishment of three distinct internal lever arm configurations for the reinforcement, hereafter referred to as layers. This variability helps in the examination of the flexural response of TRCs, considering the role of concrete cover, reinforcement location, and distances between the plies.

Two extra sets of samples were also prepared, aiming at investigating the effect of in-house coating of the textiles with mortar – samples denoted by (M) – or sand – samples denoted by (S) – on the flexural performance. For sand coating, firstly, a thin layer of epoxy resin was applied to the surface of the textiles and then left to set for one hour. A layer of sand (the same sand that was used in the concrete matrix but with particle sizes of < 0.6 mm) was then sprayed on the epoxy layer. A
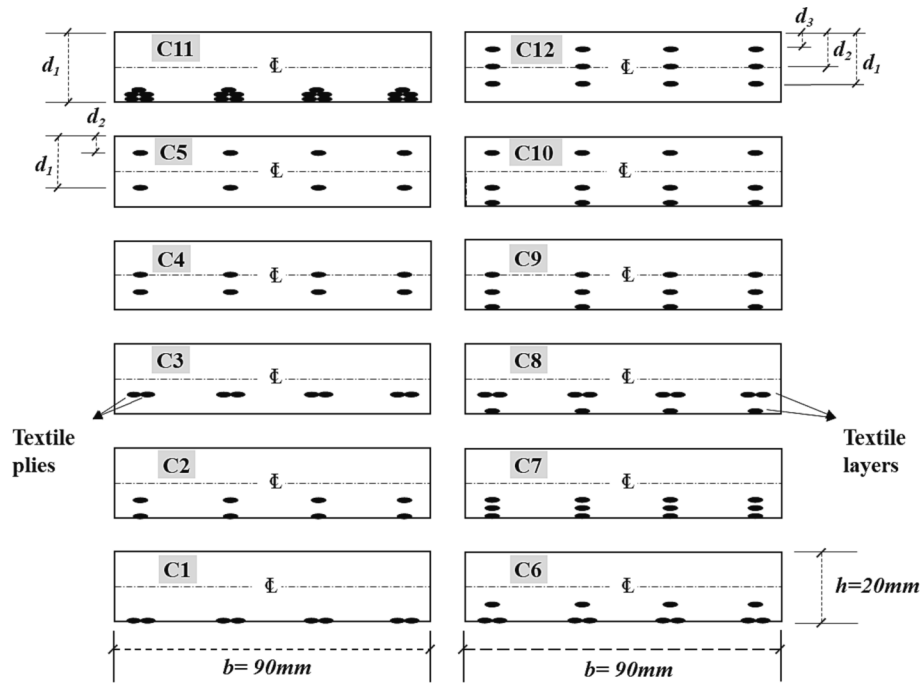
Fig. 3. Representative cross-section of the reinforcement configuration.

curing time of at least 72 hrs was adopted at room temperature for the sand-coated textile to fully dry. Mortar coating was only considered in the case of C8 samples and was attempted by immersing the textile in the same mortar used as the matrix of TRC plates prior to the casting process.

This second stage of the tests comprised 20 variables (with six identical samples for each variable) focused on the role of: (a) prestressing level presented as a percentage of the maximum tensile load of

Table 3
Tested specimens.

Sample ID	Configuration	Extra coating	No. of Plies	No. of Layers	ρ^* [%]	d1 [mm]	d2 [mm]	d3 [mm]	Prestress level [%]	Sample age [day]	Prestress release time [day]
1L0P0R28DC1	C1	–	2	1	0.37	20	20	–	0	28	–
2L0P0R28DC2	C2	–	2	2	0.37	20	15	–	0	28	–
1L0P0R28DC3	C3	–	2	1	0.37	15	15	–	0	28	–
2L0P0R28DC4	C4	–	2	2	0.37	15	10	–	0	28	–
2L0P0R28DC5	C5	–	2	2	0.37	15	5	–	0	28	–
2L0P0R28DC6	C6	–	3	2	0.56	20	20	15	0	28	–
3L0P0R28DC7	C7	–	3	3	0.56	20	17.5	15	0	28	–
2L0P0R28DC8	C8	–	3	2	0.56	20	15	15	0	28	–
2L0P0R28DC8(M)	C8	Mortar	3	2	0.56	20	15	15	0	28	–
3L0P0R28DC9	C9	–	3	3	0.56	20	15	10	0	28	–
3L0P0R28DC10	C10	–	3	3	0.56	20	15	5	0	28	–
1L0P0R28DC11	C11	–	5	1	0.93	20	–	–	0	28	–
2L0P0R7DC4B1	C4	–	2	2	0.37	10	–	15	0	7	1
2L13P1R7DC4	C4	–	2	2	0.37	10	–	15	13	7	1
2L25P1R7DC4	C4	–	2	2	0.37	10	–	15	25	7	1
2L35P1R7DC4	C4	–	2	2	0.37	10	–	15	35	7	1
2L0P0R7DC4B7	C4	–	2	2	0.37	10	–	15	0	7	7
2L13P7R7DC4	C4	–	2	2	0.37	10	–	15	13	7	7
2L35P7R7DC4	C4	–	2	2	0.37	10	–	15	35	7	7
2L0P0R28DC4B1	C4	–	2	2	0.37	10	–	15	0	28	1
2L13P1R28DC4	C4	–	2	2	0.37	10	–	15	13	28	1
2L25P1R28DC4	C4	–	2	2	0.37	10	–	15	25	28	1
2L35P1R28DC4	C4	–	2	2	0.37	10	–	15	35	28	1
3L13P1R28DC12	C12	–	3	3	0.56	10	–	15	13	28	1
2L0P0R28DC4B7	C4	–	2	2	0.37	10	–	15	0	28	7
2L13P7R28DC4	C4	–	2	2	0.37	10	–	15	13	28	7
2L35P7R28DC4	C4	–	2	2	0.37	10	–	15	35	28	7
2L0P0R28DC4B1 (S)	C4	Sand/Epoxy	2	2	0.37	10	–	15	0	28	1
2L13P1R28DC4(S)	C4	Sand/Epoxy	2	2	0.37	10	–	15	13	28	1
2L35P1R28DC4(S)	C4	Sand/Epoxy	2	2	0.37	10	–	15	35	28	1
2L13P1R90DC4	C4	–	2	2	0.37	10	–	15	13	90	1
2L35P1R90DC4	C4	–	2	2	0.37	10	–	15	35	90	1

the roving (f_{fu}), (prestressing loads of up to 0.13 f_{fu}, 0.25 f_{fu}, and 0.35 f_{fu}), (b) prestress release times (i.e. 1-day, 7-day), and (c) the age at which the specimens were tested (i.e. 7, 28, and 90 days). The selection to adopt a maximum prestressing level of 35% aligns with the American Concrete Institute recommended values for prestressed FRP tendons [45], which suggest a range of 40–65% for aramid and carbon FRP tendons. Research on the long-term creep behaviour of basalt FRP bars indicates their capability to withstand an allowable creep rupture stress of 50% of their tensile strength [46]. This choice considers the variations in bond behaviour and interfilament stress transfer between textile reinforcement and FRP tendons. All samples were reinforced using a C4 configuration in which both layers were prestressed (except in one case that was reinforced with three layers (C12), in which the top layer was non-prestressed and the two bottom layers were prestressed). The effect of sand coating on the performance of prestressed samples was also examined in a number of cases. Table 3 presents the details of both series of tested specimens.

The notation of examined specimens is xLxPxRxDCNBY(S/M), where x takes a numeric value quantifying the following inscriptions: as L refers to the number of layers (force arm), P stands for the prestress level in the percentage of the maximum tensile load of the used fabric (f_{fu}), R denotes the release time at which the prestressing force was released, D stands for the testing age of the specimens, CN presents the used reinforcement configuration, and BY is the control (Blank) samples, for the 1-day (B1) and 7-day (B7) release times. Finally, (S) indicates sand coating with epoxy, and (M) preliminary mortar coating was applied to textile reinforcement before casting.

2.4. Prestressing method

A prestressing test rig was developed as illustrated in Fig. 4. The rig was assembled on a rigid steel frame, with the textile layers being secured to a sliding clamp (**Detail "1″**) at both ends. A hydraulic jack was employed to apply the prestressing forces, which were then measured by a load cell connected to a data logger. To prevent potential stress losses resulting from the relaxation of mechanical components, control nuts were fastened at both ends of the clamp once the desired prestress level was attained. A suitable mould with separated dividing walls (see **Detail "2"**) was specifically designed to ensure the placement of the textile layers at the desired embedment depth and to enable the

production of samples with dimensions of 410 mm in length, 90 mm in width, and 20 mm in thickness. These dimensions fall above the minimum recommended values in RILEM TC 232-TDT [47].

Subsequently, the concrete mixture was poured and left to settle in order to attain adequate compressive strength before releasing the prestressing forces. At the targeted release age, the load was released, and the specimens were detached from the prestressing rig and demoulded, then subsequently cured in accordance with the prescribed curing regime. For specimens of 1-day release time, these were taken out of the prestressing rig after 24 h and subsequently immersed in a water curing tank for a duration of 7 days. Following this, they were transferred to a temperature-controlled environment maintained at 20 °C. In contrast, the specimens with a 7-day release time were covered with a polyethene sheet until they were released and then immediately placed in the same environmentally controlled storage room until the day of testing.

2.5. Flexural test set-up

The flexural response of TRC plates was determined by conducting four-point bending tests according to EN 1170-5 [48]; see Fig. 5. The tests were conducted under displacement control at a crosshead rate of 1 mm/min using a ZwickRoell machine. During the tests, the loads were
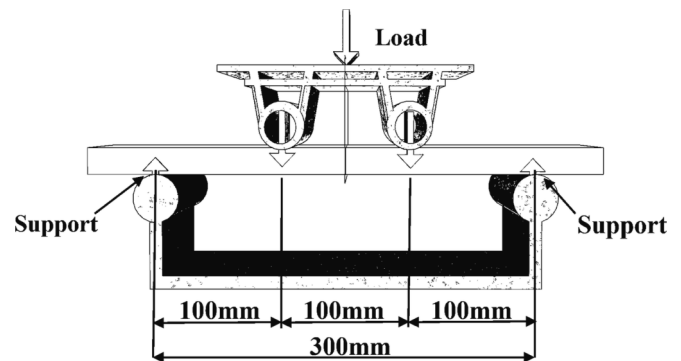
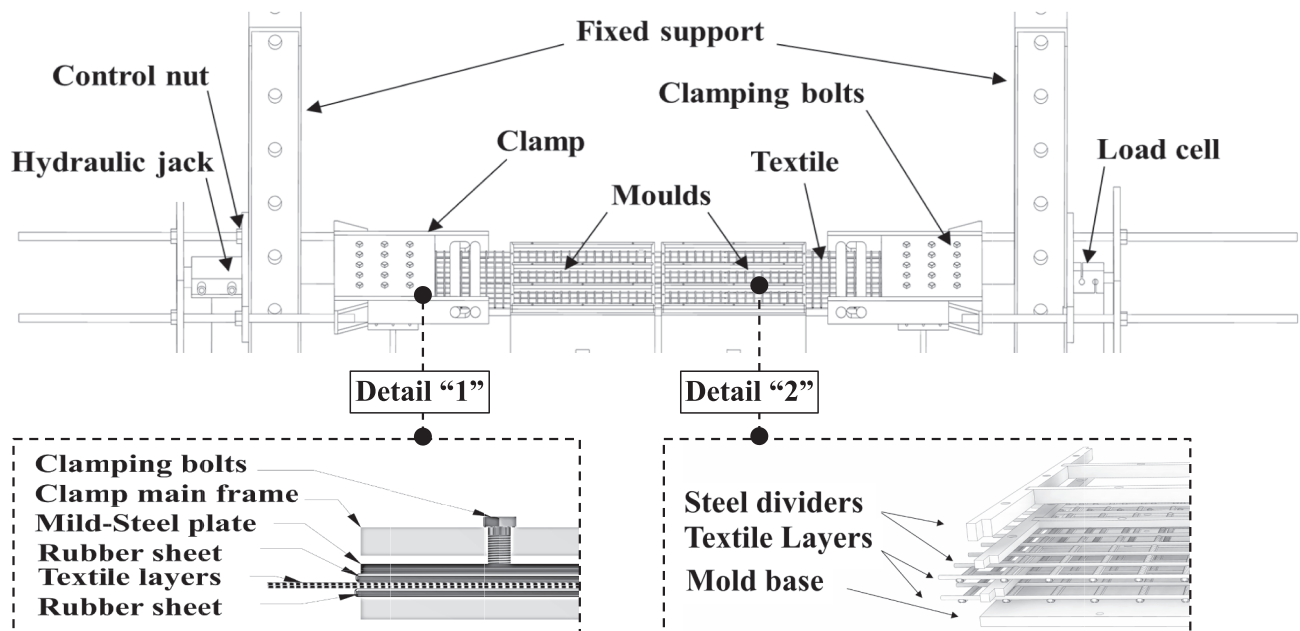**Fig. 5.** Four-point bending schematic setup.

Fig. 4. Schematic view of the proposed prestressing system.

measured using the internal load cell of the machine, and the displacements were recorded at the top quarter of samples using an Imetrum video gauge extensometer.

The experimental load (F) - displacement (δ) curves were used to calculate the flexural stress, σ, and strain, ε, at the first crack and the ultimate capacity as [48]:

$$Stress\ (\sigma) = \frac{F \times L}{b \times d^2} \tag{3}$$

$$Strain\ (\varepsilon) = \frac{27}{5} \times \frac{\delta \times d}{L^2} \tag{4}$$

where L is the span length (300 mm), b is the specimen's width (90 mm) and d is the specimen's thickness (20 mm). It is worth noting that although Eq. (4) does not provide accurate stress values after cracking of the samples, this formulation is used here to ensure consistency with the calculations reported in the literature. The initial stiffness before cracking was obtained by analysing the slope of the linear elastic region in the load–deflection curve. The flexural toughness (T) was calculated by measuring the area under the load–deflection curve up to the first crack (T_d) and up to a deflection of 10 mm (T_m) [49].

3. Results and discussion

Most of the TRC specimens exhibited the typical deformation-hardening response in both prestressed and non-prestressed samples (Fig. 6) (except for a few samples, e.g. 2L35P1R7D, which showed a strain-softening response). The overall bending behaviour can be divided into four phases [41]. In the first phase, an elastic-linear behaviour is observed, whereas the load is carried mostly by the matrix until the occurrence of the first crack. As such, the response in this phase is mainly governed by the matrix stiffness. However, factors such as the level of prestressing force, eccentricity, and interfacial bond gradually play a role in shaping the extent of this phase [50]. In the second phase, i.e. after the occurrence of the first crack, the stresses are redistributed to the textile reinforcement resulting in an abrupt drop in the stress-bearing capacity or the so-called delayed stress distribution [11], phase 2. This delay in the stress transfer is controlled by the waviness level of the yarns, reinforcement ratio (ρ) and the bond between the textile and the surrounding matrix [51,52]. With the increase in load, the sample undergoes multiple cracking as stresses are transferred by the yarns to the surrounding mortar, preventing stress localization in the initial crack. The stiffness of the samples is much lower in the second stage than in the first one. Furthermore, as the load is further increased, the neutral axis progressively shifts upwards due to ongoing

crack propagation. This shift continues until a moment equilibrium is achieved between the cracked and uncracked sections. [53]. Once the spacing between cracks becomes smaller than twice the load transfer length, a stabilised crack pattern will eventually form.

Once the crack formation is eventually stabilised, a third stage emerges, characterised by deformation hardening. This stage is characterised by a sequential increase in the stiffness, primarily governed by the reinforcement stiffness. This is accompanied by crack widening until the point of ultimate stress/failure is reached. A deformation-softening behaviour can be observed in the fourth phase, controlled mainly by the type of failure. Once the ultimate stress is reached, a sharp drop in the stress is anticipated in the event of yarn rupture as the predominant failure mode. Alternatively, a less brittle failure mode may be observed when failure is influenced by a combination of filament rupture, slippage, and compression failure of the matrix at the widened crack tip. Additionally, the occurrence of delamination failure, attributed to bond failure between the textile interface and the matrix, can also be expected. This particular failure mode results in the samples failing to reach their ultimate load capacity and inhibits the complete utilisation of the reinforcement's potential [54]. The key results obtained from both non-prestressed and prestressed samples, including first crack, ultimate stresses, toughness, and cracking behaviour, are summarised in Table 4 and discussed in the next sections.

3.1. Cracking behaviour and failure mechanism

Table 5 shows a comparison of the cracking pattern and failure mode of all tested specimens after failure, and Fig. 7 summarises the average number of cracks and saturated crack spacing observed in the specimens. The results indicate that in non-prestressed samples (Fig. 7a), an increase in the reinforcement ratio (ρ) led to a higher number of cracks and a decrease in saturated crack spacing, as expected. For instance, the incorporation of a third layer over the two-layer samples resulted in a notable increase in the average number of cracks compared to two-layer reinforced samples (e.g. 40% and 80% increase in C6 and C7 samples, respectively, is observed compared to C1-C3 samples). Similar crack densities can also be observed in samples with comparable tensile reinforcement ratios. For instance, samples C1 to C5 or samples C6-C8 showed a similar crack pattern.

In contrast, the crack spacing in specimens reinforced with three layers of textiles (i.e. C6 to C10) does not show a significant change between samples with three layers of tensile reinforcement and samples with two layers of reinforcement (e.g. C6-C8 and C9-C10). It should be noted that no delamination was observed among the samples upon examination of the failure envelope. The average crack width decreased with the increase in reinforcement ratio, as the specimens were able to withstand residual load and have lower deflection rates while having considerable damage [55]. Placing the reinforcement at high flexural depth can also result in a sudden rupture of the yarns (i.e. C1, C2) (Table 5), while the samples with lower bending depth failed due to a combination of partial filament rupture, slippage, and matrix crushing at the top caused by a higher deflection level.

In the case of prestressed samples, it was observed that the age of testing (as shown in Fig. 8b) had an insignificant influence on the quantity and distribution of cracks across all the investigated parameters. On the other hand, the density decreased slightly (and crack spacing increased slightly) with increments of prestressing loads, with a few exceptions. Prestressed samples released after 1-day typically exhibited fewer cracks at elevated prestress levels compared to their non-prestressed counterparts. Additionally, there seems to be a correlation between prestressing release day and the crack density (i.e. the crack density almost doubled in the samples released at 7-day compared to those released at 1-day), which can be the result of better bond formation in those specimens and increased effectiveness of the prestressing.

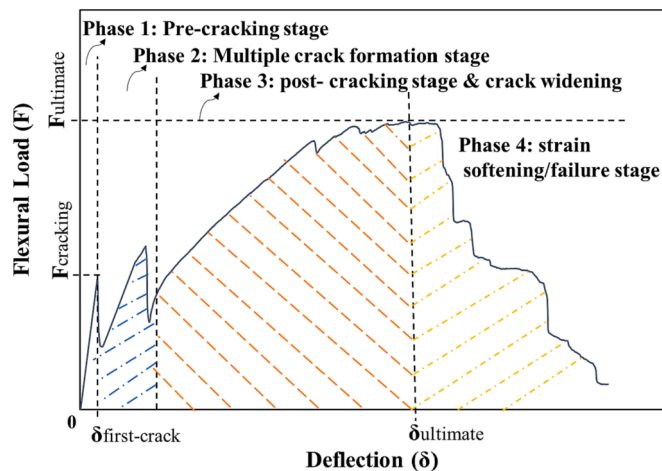Comparable results were also observed in the sand-coated samples,

Fig. 6. Typical flexural load–deflection curve of TRC plates under flexural loading.

Table 4
Summary of the flexural test results.

Sample ID	Ultimate capacity		First crack			Toughness			Cracking Behaviour
	Stress (σ$_{fu}$) [MPa]	Deflection (d$_{ult}$) [mm]	Stress (σ$_{cr}$) [MPa]	Deflection (d$_{cr}$) [mm]	Stiffness [kN/mm]	T$_{dcr}$ [kN.mm]	T$_m$ @ 10 mm [kN.mm]	No. of cracks	Crack spacing [mm]
1L0P0R28DC1	15.8(8.20)	11.2(7.20)	4.28(9.80)	0.19(25.0)	2.57(20.8)	0.07 (33.1)	12.0(8.00)	5.00(16.5)	27.0(3.23)
2L0P0R28DC2	15.7(5.20)	12.6(3.10)	4.10(11.3)	0.19(18.6)	2.44(5.88)	0.06 (31.8)	11.1(3.00)	5.00(9.32)	26.0(1.46)
1L0P0R28DC3	12.3(26.3)	12.2(18.0)	4.10(29.3)	0.19(37.0)	2.40(6.01)	0.06 (63.6)	9.10(20.6)	5.00(18.2)	26.0(1.86)
2L0P0R28DC4B1	8.30(17.0)	11.1(11.7)	3.90(19.5)	0.20(17.9)	2.32(11.8)	0.05 (27.1)	7.40(22.5)	3.00(26.3)	48.0(54.6)
2L0P0R28DC5	6.20(20.7)	8.70(10.6)	3.20 (12.15)	0.16(17.4)	2.31(36.3)	0.03 (32.8)	4.80(18.0)	2.00(22.8)	63.0(33.7)
2L0P0R28DC6	27.1(10.8)	14.2(5.90)	5.00(14.9)	0.20(12.6)	2.90(20.7)	0.07 (22.4)	17.2(11.9)	7.00(12.8)	24.0(10.2)
3L0P0R28DC7	25.0(8.60)	12.5(7.60)	4.50(18.8)	0.22(26.8)	2.55(21.2)	0.07 (44.2)	16.7(9.60)	9.00(19.9)	20.0(14.8)
2L0P0R28DC8	25.2(11.4)	12.9(6.10)	4.80(12.0)	0.22(21.0)	2.53(16.3)	0.07 (31.8)	16.8(16.2)	7.00(14.1)	24.0(12.3)
2L0P0R28DC8(M)	17.3(14.9)	8.30(29.3)	4.80(15.7)	0.18(12.8)	3.30(16.7)	0.06 (24.4)	14.1(14.0)	6.00(9.70)	25.0(7.15)
3L0P0R28DC9	21.7(9.90)	12.6(9.90)	4.70(6.00)	0.18(12.1)	3.10(12.9)	0.06 (14.8)	14.8(10.9)	8.00(14.5)	23.0(9.71)
3L0P0R28DC10	18.9(7.30)	10.3(3.50)	6.00(6.40)	0.21(10.8)	3.46(15.1)	0.08 (15.3)	14.6(8.40)	6.00(16.2)	27.0(7.99)
1L0P0R28DC11	35.5(14.6)	12.4(12.8)	5.30(11.4)	0.24(20.9)	2.64(18.3)	0.09 (28.9)	23.3(14.0)	9.00(20.7)	21.0(19.6)
2L0P0R7DC4B1	8.80(4.00)	9.35(5.50)	2.47(20.1)	0.34(6.30)	1.36(23.7)	0.07 (7.60)	7.30(11.6)	2.00(0.00)	80.0(33.0)
2L13P1R7DC4	12.2(10.1)	9.29(21.7)	6.20(9.30)	0.40(18.0)	2.47(47.0)	0.15 (23.2)	12.2(11.7)	3.00(17.3)	36.0(11.7)
2L25P1R7DC4	10.5(10.4)	13.6(5.10)	6.30(7.30)	0.37(16.4)	1.51(25.4)	0.12 (5.10)	9.60(8.00)	3.00(17.3)	33.0(15.1)
2L35P1R7DC4	7.71(7.47)	8.82(23.8)	8.60(7.60)	0.20(4.90)	4.50(6.9)	0.12 (11.2)	7.70(6.00)	2.00(0.00)	84.0(21.9)
2L0P0R7DC4B7	13.3(7.50)	11.2(22.5)	4.30(15.6)	0.20(10.8)	2.83(6.79)	0.05 (22.2)	8.50(12.5)	5.00(10.1)	27.0(3.63)
2L13P7R7DC4	16.2(8.50)	11.1(8.50)	6.60(8.80)	0.20(11.9)	3.45(8.48)	0.10 (19.0)	13.2(5.50)	5.00(12.7)	27.0(5.92)
2L35P7R7DC4	17.1(7.00)	6.20(18.0)	10.3(9.80)	0.30(8.40)	4.50(8.39)	0.18 (15.6)	16.5(5.60)	5.00(15.6)	29.0(9.23)
2L0P0R28DC4B1	8.30(17.0)	11.1(11.7)	3.90(19.5)	0.20(17.9)	2.32(11.8)	0.05 (27.1)	7.40(22.5)	3.00(26.3)	48.0(54.6)
2L13P1R28DC4	13.9(6.50)	12.6(6.60)	8.60(7.80)	0.30(10.8)	3.81(11.9)	0.14 (13.0)	12.0(3.40)	3.00(19.4)	60.0(28.5)
2L25P1R28DC4	13.7(6.20)	13.0(17.9)	9.90(9.20)	0.30(7.80)	3.83(7.53)	0.18 (15.6)	10.9(6.90)	2.00(18.8)	68.0(28.5)
2L35P1R28DC4	12.0(7.40)	13.8(25.1)	10.8(7.80)	0.30(14.2)	4.63(12.1)	0.18 (20.8)	10.1(10.7)	2.00(18.8)	89.0(21.8)
3L13P1R28DC12	13.9(10.2)	12.5(17.0)	9.90(13.4)	0.30(11.8)	3.98(4.25)	0.17 (23.5)	12.0(9.50)	2.00(22.1)	81.0(28.6)
2L0P0R28DC4B7	12.4(9.90)	12.8(7.22)	5.60(16.9)	0.20(13.7)	2.77(7.54)	0.08 (28.2)	8.90(10.6)	4.00(11.9)	31.0(16.9)
2L13P7R28DC4	17.2(5.10)	11.1(11.8)	8.10(7.30)	0.30(6.80)	3.23(5.99)	0.15 (10.3)	14.1(2.20)	5.00(15.6)	27.0(6.00)
2L35P7R28DC4	16.7(10.4)	8.22(21.7)	10.3(4.40)	0.40(5.20)	3.11(4.50)	0.28 (8.30)	16.7(6.00)	5.00(15.3)	27.0(2.60)
2L0P0R28DC4B1 (S)	17.3(11.3)	14.5(7.70)	6.80(18.3)	0.20(14.8)	3.92(7.93)	0.09 (27.6)	11.5(7.00)	5.00(30.5)	35.0(24.6)
2L13P1R28DC4(S)	18.8(10.1)	11.5(19.2)	9.90(11.6)	0.30(7.20)	4.31(12.1)	0.17 (11.3)	15.6(10.1)	4.00(22.4)	35.0(21.1)
2L35P1R28DC4(S)	18.6(11.4)	10.3(23.5)	11.2(13.2)	0.30(5.50)	4.78(10.7)	0.20 (13.2)	17.3(11.8)	5.00(18.6)	32.0(34.1)
2L13P1R90DC4	15.0(7.10)	11.9(6.3)	9.70(11.6)	0.30(14.2)	3.71(7.73)	0.19 (22.7)	12.9(5.60)	3.00(36.5)	51.0(34.9)
2L35P1R90DC4	15.1(11.9)	12.2(27.0)	12.3(8.77)	0.30(6.50)	4.66(12.9)	0.22 (17.3)	12.3(7.60)	2.00(22.3)	86.0(11.2)

*Coefficients of variation are presented in parentheses.

Table 5
Failure mechanism and crack patterns.

Sample ID	1L0P 0R28D C1	2L0P 0R28D C2	1L0P 0R28D C3	2L0P 0R7D C4B1	2L0P 0R28D C4B1	2L0P 0R7D C4B7	2L0P 0R28D C4B7	2L0P 0R28D C4B1S	2L0P 0R28D C5	2L0P 0R28D C6	3L0P0 R28D C7	2L0P 0R28D C8	3L0P 0R28D C9	3L0P 0R28D C10	1L0P 0R28D C11
Failure mode	F.R	F.R	P.R	C.C/ P.R	C.C/ P.R	C.C/ P.R	C.C/ P.R	F.R	C.C/ P.R	P.R	P.R	P.R	P.R	P.R	P.R
Non-prestressed plates															

Sample ID	2L13P 1R7D C4	2L25P 1R7D C4	2L35P 1R7D C4	2L13P 7R7D C4	2L35P 7R7D C4	2L13P 1R28D C4	2L25P 1R28D C4	2L35P 1R28D C4	3L13P 1R28D C12	2L13P 7R28D C4	2L35P 7R28D C4	2L13P 1R28D C4(S)	2L35P 1R28D C4(S)	2L13P 1R90D C4	2L35P 1R90D C4
Failure mode	C.C/ P.R	C.C/ P.R	C.C/ F.S	P.R	P.R	C.C/ P.R	C.C/ P.R	C.C	C.C/ P.R	P.R	P.R	P.R	P.R	P.R	P.R
Prestressed plates															

C.C.: Concrete crushing; F.R.: Full fabric rupture; P.R: Partial fabric rupture; F.S: Fabric slippage.
C.C/F.R/P.R/ F.S: Combined concrete crushing with full fabric rupture, partial fabric rupture and fabric slippage.
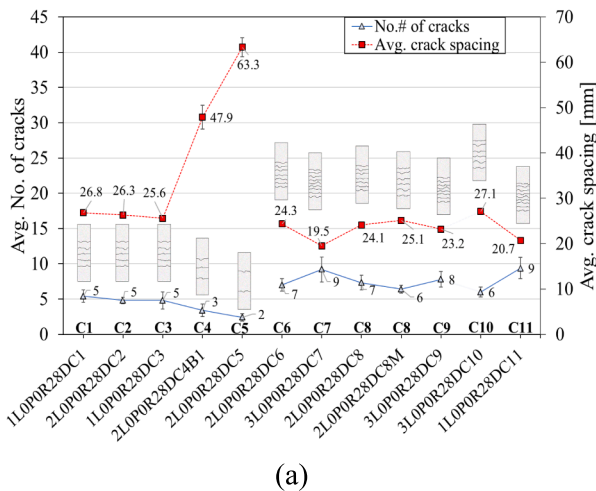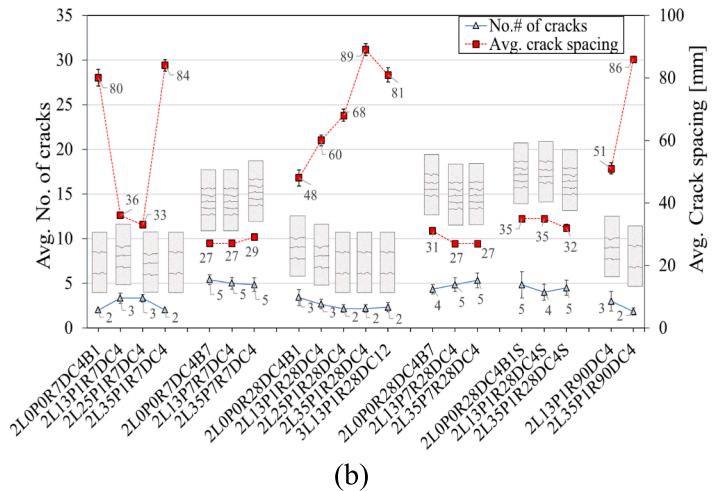
Fig. 7. Average number of cracks and their average spacing: a) non-prestressed plates; b) prestressed plates.

wherein the incorporation of an additional sand coating led to a denser crack formation. A substantial increase of 70% in crack density was observed over the samples released at 1-day. This increase can be attributed to the improved bond strength in sand coated samples. This enhancement resulted in a more effective utilisation of the textile's tensile strength, whereas the sand-coated samples exhibited failure due to complete yarn rupture. The application of a sand coating contributed to this improved bond strength and subsequently led to an enhancement in the overall stiffness of the composite material [27]. Prestressing led to a more brittle failure, as the prestressed samples mainly failed by rupture of the yarns (Table 5). When all filaments within the textile reinforcement are fully activated and their tensile strength is effectively utilised, it is anticipated that a more homogeneous stress distribution will occur. However, this also tends to result in more brittle behaviour. This brittleness became more apparent in the sand-coated samples and the samples released at 7-day, while the age of testing had no significant effect on the failure mechanism of the samples.

3.2. Flexural behaviour - non-prestressed TRC plates

The change in the flexural behaviour of non-prestressed samples with reinforcement configuration (flexural depth, reinforcement ratio) is presented in Fig. 8. Fig. 8a shows a comparison between samples with different tensile reinforcement ratios (0.37%, 0.56% and 0.93%, C1, C6,
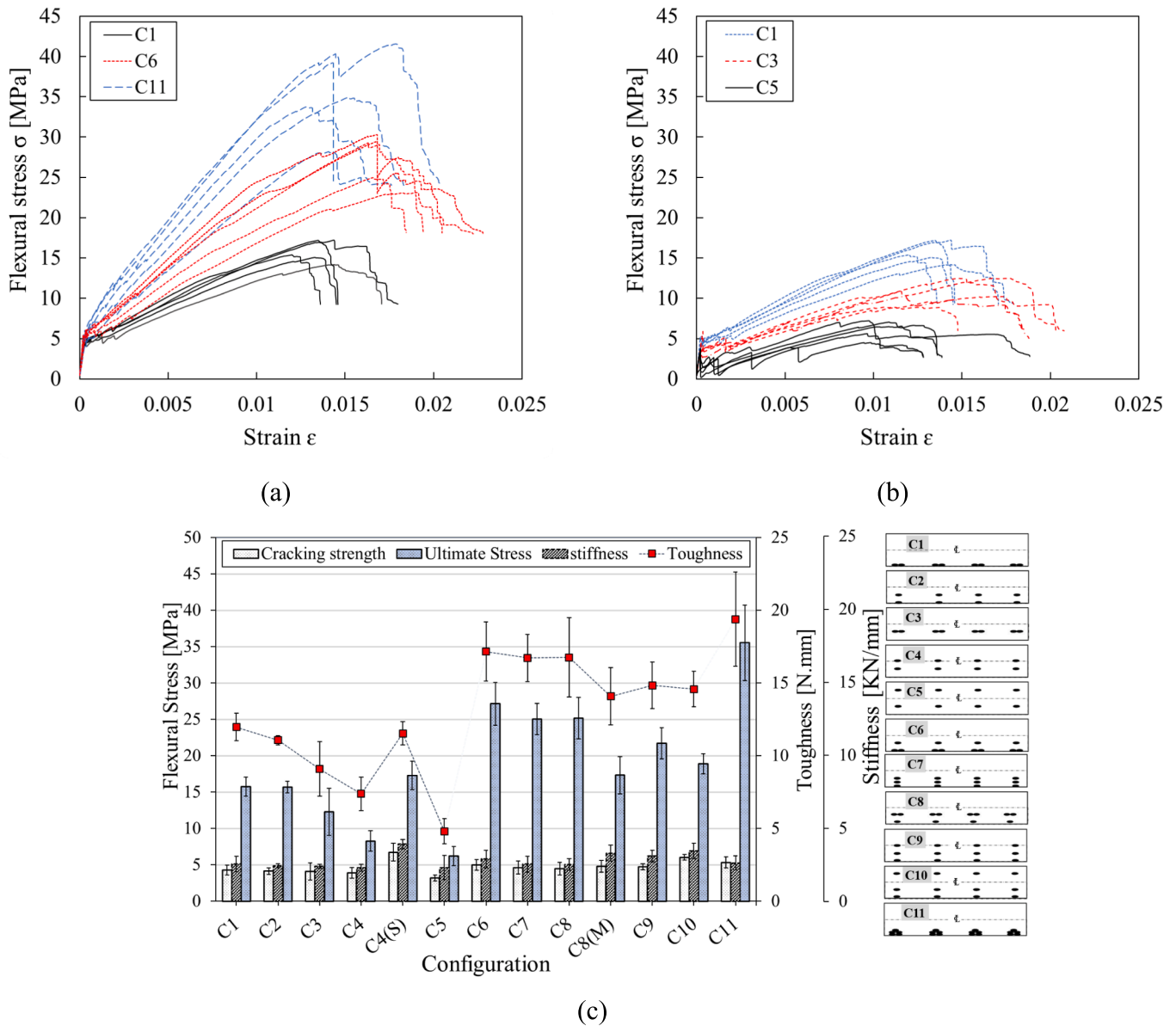
(a)

(b)

(c)

Fig. 8. Non-prestressed TRC plates: a) flexural stress–strain curves with different reinforcement ratios; b) flexural stress–strain curves with different configurations; c) comparison of First Crack Stress, Pre-cracking Stiffness, Ultimate Stress, and Toughness at 10 mm deflection (T_m) of different reinforcement configurations.

and C11, respectively) and a similar reinforcement depth. It can be seen that the reinforcement ratio did not have a significant influence on the flexural cracking stress, stiffness, or toughness at the pre-cracking stage (Phase1). However, its effect on the post-cracking (Phase 3) stiffness and strength is evident; these increase by increasing the reinforcement ratio as the member response is mainly governed by the textile in this stage [56]. In the case of samples where the textile layers were positioned closer to the neutral axis (e.g. C5) (Fig. 8b), a noticeable delay in textile activation was observed, characterised by a sharp decrease in stress following cracking. As the reinforcement depth increased, i.e. in C3 and C1, and the reinforcement ratio increased, i.e. in C6 and C11, this drop in stress (delay) became less pronounced. However, the reinforcement ratio had only a minor influence on the ultimate deflection, resulting in a negligible increase.

The results indicate a positive relationship between the reinforcement ratio and both the ultimate stress and toughness (T_m) of the samples (see C1, C6, and C11), as demonstrated in Fig. 8b. Comparing the C6 and C1 samples, it is evident that a 50% increase in the reinforcement ratio resulted in a substantial 70% enhancement in flexural stress and a

44% improvement in flexural toughness at 10 mm deflection (T_m). However, this enhancement became less significant after exceeding a certain level of reinforcement ratio. Increasing the reinforcement ratio by 65% in C11 samples over C6 samples has only led to a further improvement of 31% and 36% in flexural stress and toughness, respectively.

The influence of the flexural depth of the tensile reinforcement is insignificant on the cracking stress, stiffness, and toughness (T_{dcr}) of the specimens prior to cracking, but more notable on the flexural strength or toughness at 10 mm (T_m), see C1-C3 or C6-C8 in Fig. 8c and Table 4. However, when one of the layers was positioned at or above the neutral axis (e.g. in C4 and C5 or C9 and C10), a slight reduction in the cracking stress and toughness (T_{dcr}) and a more notable reduction in the flexural strength or toughness at 10 mm (T_m) was observed. The role of adding reinforcement in the compression zone can be observed by comparing C2 and C10 samples. A slight increase in cracking stress and stiffness can be observed, with a more significant increase in the ultimate strength and toughness (T_m), (20% and 32% increase, respectively), and a decrease in the ultimate deflection (20%), with no evident effect on

changing the failure mechanism. Moreover, within the same set of samples (C1-C5), C1 and C2 configurations demonstrated nearly identical mechanical properties, exhibiting the highest stiffness and flexural stress, as illustrated in Fig. 8c.

The non-prestressed sand-coated samples demonstrated a significant improvement in various mechanical properties in comparison to their non-prestressed polymer-coated counterparts, as anticipated (see Fig. 8c). The incorporation of a sand coating in C4(S) increased the cracking stress and stiffness by 75% and 69%, respectively. Furthermore, it led to a significant enhancement of 55% in flexural toughness (T_m), 108% in ultimate flexural stress, and a 30% increase in deflection when compared to the samples without sand coating (C4). The utilisation of the textile tensile strength was demonstrated by the change in the sample's failure mode, where it changed from partial rupture of the yarns in non-coated samples to a complete rupture of the yarns in sand-coated samples. These improvements can be attributed to the enhanced bond of sand-coated yarns with the matrix and the increased thickness of the resin layer when combined with sand [12,57–59]. Furthermore, the mortar-coated samples (C8M) scored the lowest flexural strength (30%

less) and toughness (16% less) but had similar pre-cracking properties compared to the counterpart samples of the same configuration but without extra coating (C8). This can be related to the poor bond caused by the time-lapse between the thin coating layer and the newly placed concrete, but it needs to be further investigated in future studies.

3.3. Flexural behaviour - prestressed TRC plates

3.3.1. Role of prestressing level and release time

Fig. 9 presents the typical flexural stress–strain curves and a summary of all the results of prestressed TRC samples with 1-day and 7-day release times. The samples were all tested at the age of 28 days to allow comparisons. It is notable that prestressing level have a significant effect in improving the flexural characteristics of the tested specimens.

Prestressing of TRC samples had a variant effect on their ultimate deflection in correspondence to the release time. The 1-day released specimens exhibited an increase in the ultimate deflection with an increase in the prestress level (Fig. 9a and Table 4). In contrast, the 7-day released specimens showed a decrease in the ultimate deflection
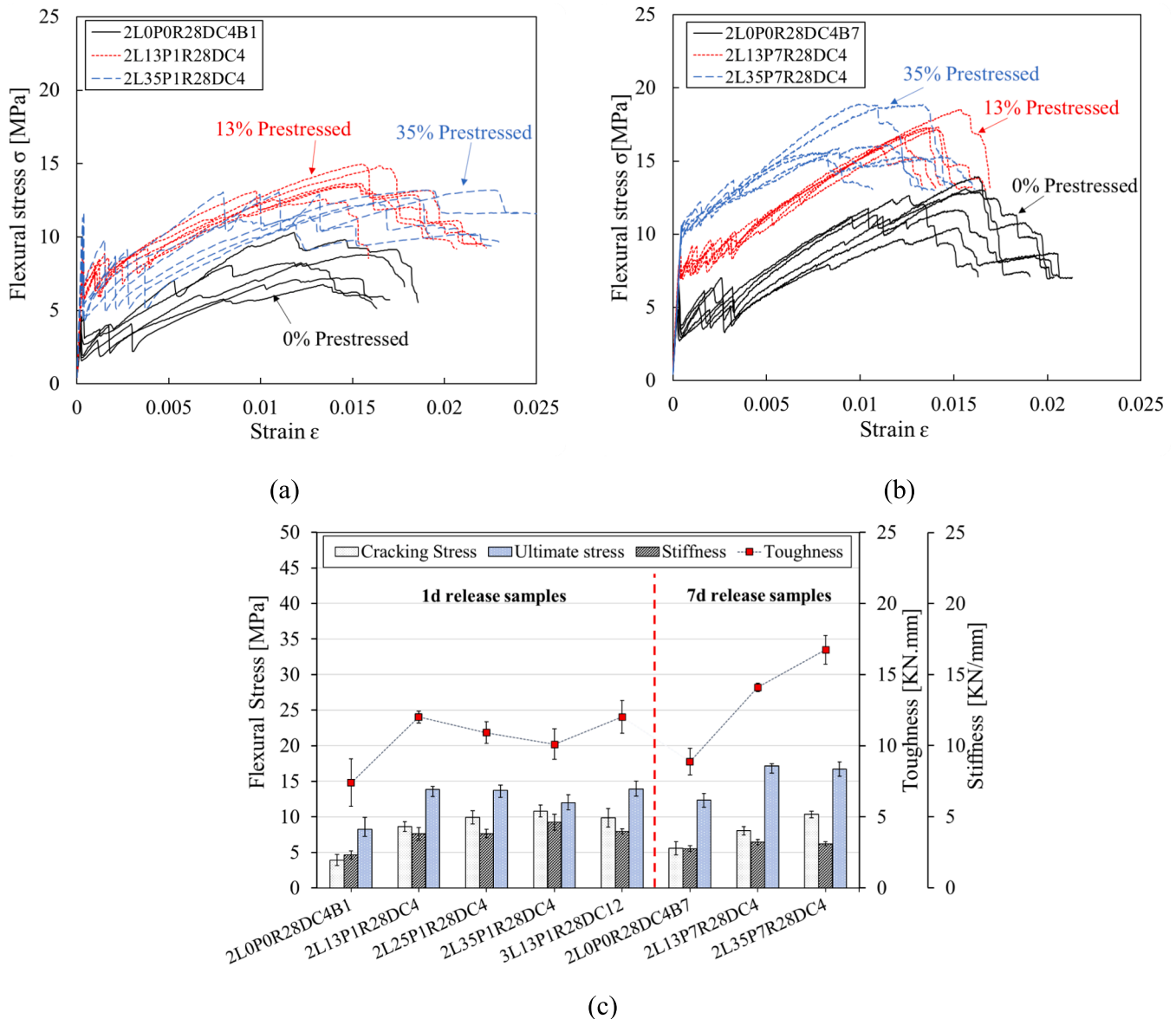

(a)

(b)

(c)

Fig. 9. Role of prestressing level and release time: a) flexural stress–strain curves at 1-day release time; b) Flexural stress–strain curves at 7-day release time; and c) comparison of First Crack Stress, Pre-cracking Stiffness, Ultimate Stress, and Toughness at 10 mm deflection (T_m).

(Fig. 9b). This phenomenon can be attributed to the influence of the release time on bond behaviour, although it has yet to be verified. Similar patterns have been noted in existing literature concerning the impact of prestressing on ultimate deflection [27,30,60]. These variations can be attributed to differences in production methods, particularly in terms of prestressing levels, release times the materials employed, and the resulting bond behaviour. Additionally, while no significant change in the stress transfer mechanisms and stress distribution delay with prestressing is observed in 1-day released specimens, there is a clear effect in 7-day released samples.

It can be observed that there is an increase in the first cracking stress with an increase in the level of prestressing in both the 1-day and 7-day released samples (Fig. 9c). At a prestress level of 35%, this increment reaches up to 176% and 83% for the 1-day and 7-day samples, respectively. Furthermore, the specimens exhibited stiffer behaviour, particularly in the 1-day released specimens. At a prestress level of 13%, the pre-cracking stiffness increases by 65%, which doubles when the prestress level is increased to 35%. This increment in pre-cracking stiffness was comparatively less prominent in the 7-day released samples, with an increase of only 16% and 12% at prestress levels of 13% and 35%, respectively.

In the 1-day released specimens, an increase in both toughness and ultimate flexural stress is observed with an increase in prestress level to 13%, with a significant increment of 67%. However, a slight decrease is observed when the prestress level is further increased to 25%, although the values remain higher than those of the reference samples (Fig. 9c). In the specimens released at 7-day, a similar change in the ultimate flexural stress is observed, the strength increased until 13% prestressing level and then remained constant at higher prestress levels. The toughness, however, increases with increasing the prestress levels in these samples. It can also be observed that adding one layer of non-prestressed textile in the compression zone, 3L13P1R28DC12, had no evident effect on the flexural performance of the prestressed samples compared to its identical samples which only consisted of two layers of tensile reinforcement, 2L13P1R28DC4.

3.3.2. Role of surface modification

The effect of sand coating on the flexural response of prestressed samples is presented in Fig. 10 and Table 4. Upon inspection of the stress–strain curves of the sand-coated samples (as depicted in Fig. 10a), it's notable that prestressing of sand-coated textiles has improved their flexural properties when compared to their control samples. However, the application of prestressing to the samples resulted in a decrease of ultimate deflection by 21% and 29% in 2L131R28DC4(S) and 2L351R28DC4(S), respectively, compared to their respective non-prestressed control samples (2L0P0R28DC4B1(S)).

In prestressed samples, the influence of sand coating on the initial cracking stress and pre-cracking stiffness was comparatively insignificant, whereas it had a more pronounced impact on the ultimate stress and toughness at 10 mm (T_m) in comparison to the samples with a polymer coating (Fig. 10b). For instance, for a prestress level of 13%, the cracking strength and pre-cracking stiffness of specimens 2L13P1R28DC4(S) showed only a 14% increase as compared to 2L13P1R28DC4. Conversely, the ultimate stress and toughness (T_m) showed a more substantial increase of 35% and 30%, respectively. Furthermore, sand-coated specimens with a prestressing level of 35% (i. e. 2L351R28DC4(S)) displayed almost identical values of cracking stress and stiffness as those without sand-coating (i.e. 2L35P1R28DC4). Nonetheless, the ultimate stress and toughness (T_m) values exhibited a more significant increase, respectively, of 50% and 70%. Where the sand-coated samples ultimately had similar flexural strength values at all prestress levels.

3.3.3. Role of testing age

The changes in the flexural response of prestressed specimens with age (7, 28, and 90 days) are shown in Fig. 11, and the results are summarised in Fig. 12. It can be observed that specimens subjected to lower levels of prestress, specifically at 13% (Fig. 11a), do not show a significant change in flexural properties with age, particularly with regards to ultimate stress and deflection with a strain-hardening trend. Conversely, for specimens subjected to a 35% prestress level (Fig. 11b), it was observed that full utilisation of the prestressing effect required a longer duration (i.e. more than 28 days). This can be due to the combined effect of high prestressing loads, insufficient bond strength, and low concrete stiffness at an early age in specimens subjected to a 35% prestress level. It is interesting to note that these samples show a similar flexural response at the age of 90 days to those loaded at 13%.

Among the samples examined, the impact of testing age is most prominently evident in the 1-day released samples (see Fig. 12a). At low prestress levels (i.e. 13%), the samples gained 80% of their ultimate flexural stress and toughness (T_m) within the first seven days, while the cracking stress and pre-cracking stiffness required a longer period to
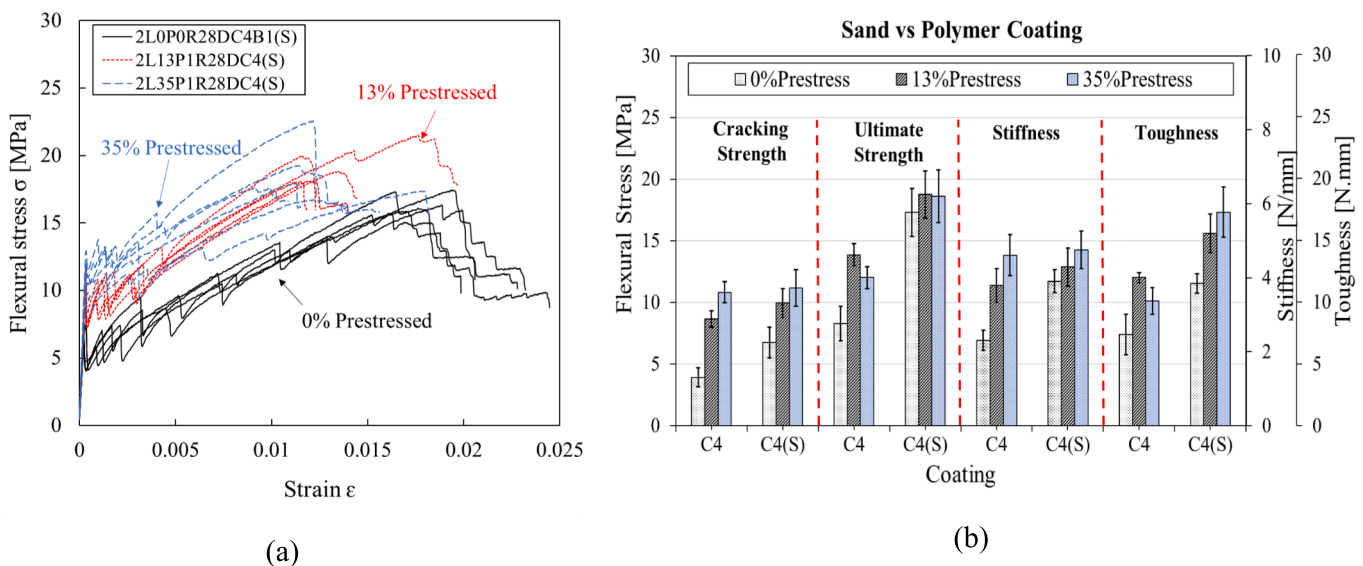

Fig. 10. Role of surface modification: a) flexural stress–strain curves of sand-coated prestressed samples at different prestress levels; b) comparison of First Crack Stress, Pre-cracking Stiffness, Ultimate Stress, and Toughness at 10 mm deflection (T_m) between samples with and without additional sand coating.
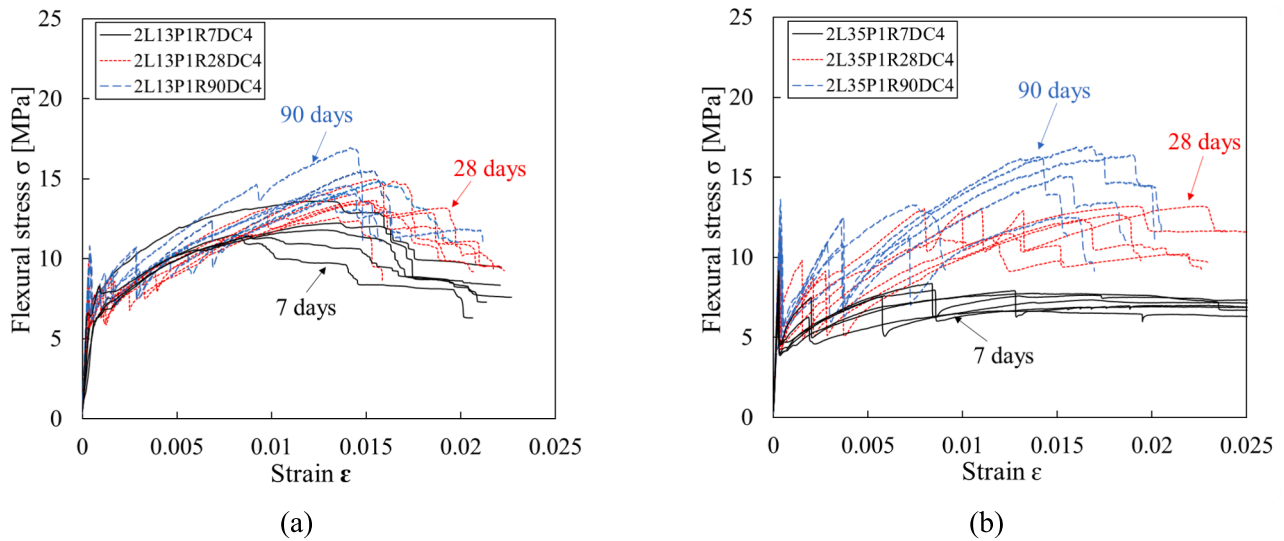
Fig. 11. Role of testing age: a) flexural stress–strain curves for prestressed specimens at 13% prestress level; b) flexural stress–strain curves at 35% prestress level.
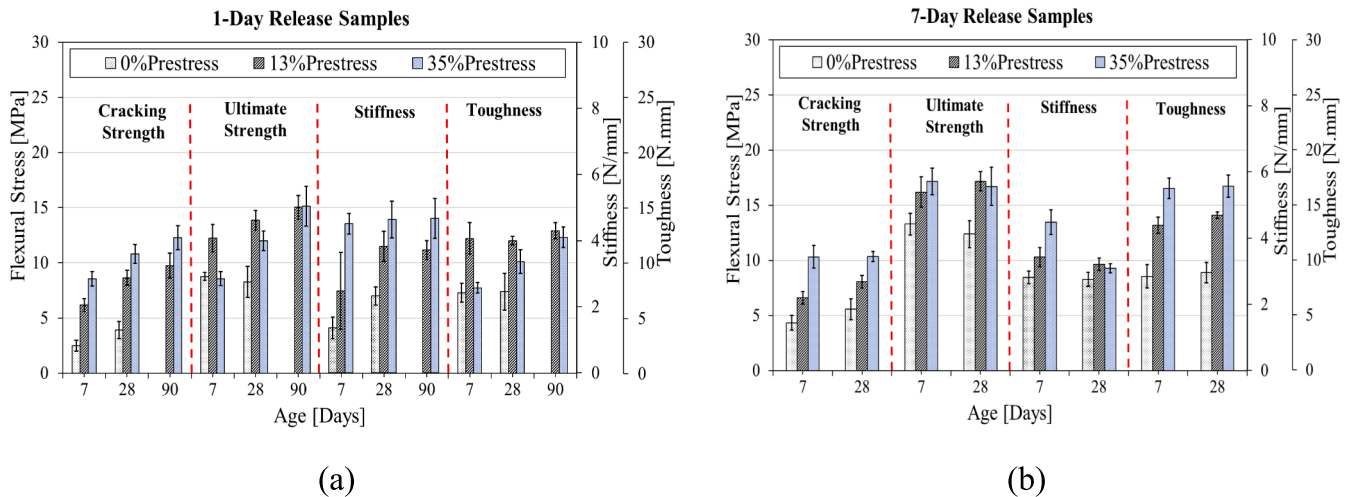

Fig. 12. Role of testing age: comparison of First Crack Stress, Pre-cracking Stiffness, Ultimate Stress, and Toughness (T_m) at: a) 1-day release time; b) 7-day release time.

develop. The samples tested at 28 days (designated as 2L13P1R28DC4) exhibited a notable enhancement of 39% in cracking stress and 54% in pre-cracking stiffness compared to their prestressed counterparts tested at seven days (designated as 2L13P1R7DC4). At the age of 90 days, the samples demonstrated a further 14% improvement in terms of cracking stress. However, the pre-cracking stiffness did not change significantly. In contrast, samples with a higher prestress level (i.e. 35%) reached most of their cracking stress and pre-cracking stiffness in the first seven days. A progressive enhancement of other flexural characteristics occurred until 90 days. Specifically, the flexural strength and toughness (T_m) development took longer, with an increase of 56% and 32% over the 28-day period, followed by a further 26% and 22% improvement until 90 days, respectively. This disparity can be attributed to the larger prestress losses experienced at higher levels of prestressing.

Contrary to the 1-day release samples, the effect of testing age was comparatively less significant in the 7-day released samples (Fig. 12b). This indicates that 7-day released samples developed most of their flexural characteristics within the first seven days of their age. Specifically, when considering a prestressing level of 13%, samples tested at 28 days (i.e. 2L13P7R28DC4) showed a slight reduction in the pre-cracking stiffness and only a 23% increase in the cracking stress

compared to those tested at seven days (i.e. 2L13P7R7DC4). Furthermore, an insignificant increase of 6% and 7% was noted in the ultimate strength and toughness (T_m), respectively. In contrast, for the specimens with a prestress level of 35%, the cracking stress, ultimate stress, and toughness (T_m) values remained constant, with a 30% decrease in pre-cracking stiffness in 2L35P7R28DC4 at 28 days of age when compared to those tested at seven days.

4. Conclusions

A systematic investigation of the flexural behaviour of non-prestressed and prestressed basalt-based TRC flat thin slabs with different reinforcement configurations was presented in this paper. The flexural response of the TRC slabs was presented and discussed in terms of stress–strain curves, flexural toughness, failure mechanism, and cracking behaviour. The experimental observations led to the following conclusions:

1- Increasing the reinforcement ratio and depth improved bearing capacity and crack density. An increase in the composite toughness and a reduction in the composite brittle failure resulted from higher

reinforcement ratios. Increased reinforcement depth led to better utilisation of textile tensile strength, which led to increased brittle failure caused by a complete textile rupture. Failure modes generally involved full and partial filament rupture, concrete crushing, and no delamination.

2- Prestress release time significantly affected the flexural response, especially at higher prestress levels. Recommended prestressing levels of up to 25% of ultimate tensile load were identified for a 1-day release time. Higher prestress levels are attainable with longer release times, subject to a maximum permissible level of 0.35 f_{fu} to prevent filament overstressing. Delayed release led to denser crack patterns with increased cracks and reduced spacing.

3- Textile surface modification yielded remarkable improvements, enhancing first crack load, flexural strength, stiffness, and toughness, while significantly reducing ultimate deflection. Additionally, an extra sand coat notably improved cracking behaviour by increasing crack count and reducing spacing.

4- The age of specimens was substantial to fully utilise the effect of prestressing at higher levels on the ultimate stress, especially in the samples released at 1-day. It was observed that the increase of the ultimate flexural stress at different prestress levels eventually reached a certain level to have equal values at all prestress levels, while the timing of its development depended on the investigated variables. Further study is needed to determine the reason behind this behaviour.

5- The application of prestressing has been demonstrated to enhance the flexural performance of PTRC, with compression stresses from prestressed reinforcement improving cracking strength, stiffness, toughness, and ultimate bearing capacity.

It's essential to note that these benefits depend significantly on production techniques, demanding careful consideration and implementation. Further research is still needed to investigate the bond behaviour, measurements of time-dependent prestress losses, and effects of creep and relaxation, on the structural behaviour of the investigated parameters in this work.

CRediT authorship contribution statement

Mohammed Hutaibat: Writing – review & editing, Writing – original draft, Visualization, Validation, Methodology, Investigation, Formal analysis, Data curation, Conceptualization. **Bahman Ghiassi:** Writing – review & editing, Validation, Supervision, Project administration, Funding acquisition, Conceptualization. **Walid Tizani:** Writing – review & editing, Validation, Supervision.

Declaration of Competing Interest

The authors declare that they have no known competing financial interests or personal relationships that could have appeared to influence the work reported in this paper.

Data availability

Data will be made available on request.

References

[1] C. Cherif, Textile Materials for Lightweight Constructions: Technologies - Methods - Materials - Properties, Springer Berlin Heidelberg2015, https://doi.org/10.1007/978-3-662-46341-3.

[2] A. Peled, B. Mobasher, Tensile behavior of fabric cement-based composites: pultruded and cast, J. Mater. Civ. Eng. 19 (4) (2007) 340–348, https://doi.org/10.1061/(ASCE)0899-1561(2007)19:4(340).

[3] E. Sharei, A. Scholzen, J. Hegger, R. Chudoba, Structural behavior of a lightweight, textile-reinforced concrete barrel vault shell, Compos. Struct. 171 (2017) 505–514, https://doi.org/10.1016/j.compstruct.2017.03.069.

[4] B. Kromoser, P. Preinstorfer, J. Kollegger, Building lightweight structures with carbon-fiber-reinforced polymer-reinforced ultra-high-performance concrete: Research approach, construction materials, and conceptual design of three building components, Struct. Concr. 20 (2) (2019) 730–744, https://doi.org/10.1002/suco.201700225.

[5] A. Dalalbashi, B. Ghiassi, D.V. Oliveira, A multi-level investigation on the mechanical response of TRM-strengthened masonry, Mater. Struct. 54 (6) (2021) 224, https://doi.org/10.1617/s11527-021-01817-4.

[6] N.R.T.M. Edoardo Rossi, H. Peter, Flexural Strengthening with Fiber-/Textile-Reinforced Concrete, ACI Struct. J. 118 (4) (2021). https://doi.org/10.14359/51732647.

[7] E. Giordano, M.G. Masciotta, F. Clementi, B. Ghiassi, Numerical prediction of the mechanical behavior of TRM composites and TRM-strengthened masonry panels, Constr. Build. Mater. 397 (2023), 132376, https://doi.org/10.1016/j.conbuildmat.2023.132376.

[8] F. Monni, E. Quagliarini, S. Lenci, F. Clementi, Dry Masonry Strenghtening through Basalt Fibre Ropes: Experimental Results against Out-of-Plane Actions, Key Eng. Mater. 624 (2015) 584–594.

[9] M. K, S. K, Sustainable performance criteria for prefabrication construction system, Int. J. Sci. Res. Publ. (IJSRP) 10 (4) (2020) p10052.

[10] J. Hegger, S. Voss, Investigations on the bearing behaviour and application potential of textile reinforced concrete, Eng. Struct. 30 (7) (2008) 2050–2056, https://doi.org/10.1016/j.engstruct.2008.01.006.

[11] N. Williams Portal, L. Nyholm Thrane, K. Lundgren, Flexural behaviour of textile reinforced concrete composites: experimental and numerical evaluation, Mater. Struct. 50 (1) (2017).

[12] K. Botelho Goliath, D.C. T. Cardoso, F. de A. Silva, Flexural behavior of carbon-textile-reinforced concrete I-section beams, Compos. Struct. 260 (2021) 113540.

[13] K. Holschemacher, Application of innovative materials in precast concrete structures. Proceedings of International Structural Engineering and Construction 4 (2017), https://doi.org/10.14455/ISEC.res.2017.106.

[14] M. Kurban, O. Babaarslan, İ.H. Çağatay, Investigation of the flexural behavior of textile reinforced concrete with braiding yarn structure, Constr. Build. Mater. 334 (2022), 127434, https://doi.org/10.1016/j.conbuildmat.2022.127434.

[15] I.G. Colombo, A. Magri, G. Zani, M. Colombo, M. di Prisco, Textile Reinforced Concrete: experimental investigation on design parameters, Mater. Struct. 46 (11) (2013) 1933–1951, https://doi.org/10.1617/s11527-013-0017-5.

[16] C.M. Cruz, U. Gohil, T. Quadflieg, T. Gries, M. Raupach, Improving the bond behavior of textile reinforcement and mortar through surface modification, 2015.

[17] S. Xu, M. Krüger, H.-W. Reinhardt, J. Ožbolt, Bond Characteristics of Carbon, Alkali Resistant Glass, and Aramid Textiles in Mortar, J. Mater. Civ. Eng. 16 (4) (2004) 356–364, https://doi.org/10.1061/(ASCE)0899-1561(2004)16:4(356).

[18] C. Morales Cruz, M. Raupach, M.G. Grantham, C. Mircea, Influence of the surface modification by sanding of carbon textile reinforcements on the bond and load-bearing behavior of textile reinforced concrete, MATEC Web Conf. 289 (2019) 04006.

[19] M. Schleser, B. Walk-Lauffer, M. Raupach, U. Dilthey, Application of Polymers to Textile-Reinforced Concrete, J. Mater. Civ. Eng. 18 (5) (2006) 670–676, https://doi.org/10.1061/(ASCE)0899-1561(2006)18:5(67.

[20] J. Donnini, V. Corinaldesi, A. Nanni, Mechanical properties of FRCM using carbon fabrics with different coating treatments, Compos. B Eng. 88 (2016) 220–228, https://doi.org/10.1016/j.compositesb.2015.11.012.

[21] B. Li, H. Xiong, J. Jiang, X. Dou, Tensile behavior of basalt textile grid reinforced Engineering Cementitious Composite, Compos. B Eng. 156 (2019) 185–200, https://doi.org/10.1016/j.compositesb.2018.08.059.

[22] R. Barhum, V. Mechtcherine, Influence of short dispersed and short integral glass fibres on the mechanical behaviour of textile-reinforced concrete, Mater. Struct. 46 (4) (2013) 557–572, https://doi.org/10.1617/s11527-012-9913-3.

[23] J. Schmidt, A. Bennitz, P. Goltermann, D.L. Ravn, External post-tensioning of CFRP tendons using integrated sleeve-wedge anchorage, Proceedings of the 6th International Conference on FRP Composites in Civil Engineering, CICE 2012 (2012).

[24] K. Zdanowicz, R. Kotynia, S. Marx, Prestressing concrete members with fibre-reinforced polymer reinforcement: State of research, Struct. Concr. 20 (3) (2019) 872–885.

[25] J.P. Osman Letelier, A. Hueckler, M. Schlaich, Application of Prestressed CFRP Textiles for the Development of Thin- Walled Concrete Structural, Elements (2019) 102–109, https://doi.org/10.2749/newyork.2019.0102.

[26] A. Peled, Pre-tensioning of fabrics in cement-based composites, Cem. Concr. Res. 37 (2007) 805–813, https://doi.org/10.1016/j.cemconres.2007.02.010.

[27] M. Krüger, Vorgespannter textilbewehrter Beton (Prestressed textile reinforced concrete), Philosophy doctoral thesis, Stuttgart, Universität Stuttgart, Fakultät Bau- und Umweltingenieurwissenschaften, Diss, 2004, https://doi.org/10.18419/opus-192.

[28] H.W. Reinhardt, M. Krüger, C.U. Große, Concrete Prestressed with Textile Fabric, J. Adv. Concr. Technol. 1 (3) (2003) 231–239, https://doi.org/10.3151/jact.1.231.

[29] Y. Du, X. Zhang, L. Liu, F. Zhou, D. Zhu, W. Pan, Flexural Behaviour of Carbon Textile-Reinforced Concrete with Prestress and Steel Fibres, Polymers 10 (1) (2018) 98, https://doi.org/10.3390/polym10010098.

[30] Y. Du, X. Zhang, F. Zhou, D. Zhu, M. Zhang, W. Pan, Flexural behavior of basalt textile-reinforced concrete, Constr. Build. Mater. 183 (2018) 7–21, https://doi.org/10.1016/j.conbuildmat.2018.06.165.

[31] C. Meyer, G. Vilkner, Glass Concrete Thin Sheets Prestressed with Aramid Fiber Mesh, PRO 30: 4th International RILEM Workshop on High Performance Fiber Reinforced Cement Composites (HPFRCC 4), RILEM Publications, 2003, p. 325.

[32] G. Vilkner, Glass concrete thin sheets reinforced with prestressed aramid fabrics, Columbia University, 2004.

[33] C.W. Dolan, H.R.T. Hamilton, C.E. Bakis, A. Nanni, Design Recommendations for Concrete Structures Prestressed with FRP Tendons. Volume 1, 2001.

[34] P. Purnell, The durability of glass fibre reinforced cements made with new cementitious matrices, 1998.

[35] E. Monaldo, F. Nerilli, G. Vairo, Basalt-based fiber-reinforced materials and structural applications in civil engineering, Compos. Struct. 214 (2019) 246–263, https://doi.org/10.1016/j.compstruct.2019.02.002.

[36] Ramakrishnan, N.S. Tolmare, V.B. Brik, Performance Evaluation of 3-D Basalt Fiber Reinforced Concrete & Basalt Rod Reinforced Concrete NCHRP-IDEA Program Project Final Report (1998).

[37] T. Bhat, V. Chevali, X. Liu, S. Feih, A.P. Mouritz, Fire structural resistance of basalt fibre composite, Compos. A Appl. Sci. Manuf. 71 (2015) 107–115, https://doi.org/10.1016/j.compositesa.2015.01.006.

[38] B. Wei, H. Cao, S. Song, RETRACTED: Environmental resistance and mechanical performance of basalt and glass fibers, Mater. Sci. Eng. A 527 (2010) 4708–4715, https://doi.org/10.1016/j.msea.2010.04.021.

[39] J. Golaszewski, G. Cygan, M. Golaszewska, Development and Optimization of High Early Strength Concrete Mix Design, IOP Conf. Ser. Mater. Sci. Eng. 471 (2019), 112026, https://doi.org/10.1088/1757-899x/471/11/112026.

[40] C. Dolan, H. Hamilton, Prestressed Concrete: Building, Design, and Construction, 2019, https://doi.org/10.1007/978-3-319-97882-6.

[41] W. Brameshuber, State-of-the-art report of RILEM technical committee TC 201-TRC Textile reinforced concrete, Bagneux : RILEM2006.

[42] British Standards Institution (2011) BS EN 197-1:2011. Cement: Composition, specifications and conformity criteria for common cements., British Standards Institution, London, 2011.

[43] ASTM C109 / C109M-16a, Standard Test Method for Compressive Strength of Hydraulic Cement Mortars (Using 2-in. or [50-mm] Cube Specimens), ASTM International, West Conshohocken, PA, 2016., www.astm.org.

[44] M.S. Choi, J.S. Lee, K.S. Ryu, K.-T. Koh, S.H. Kwon, Estimation of rheological properties of UHPC using mini slump test, Constr. Build. Mater. 106 (2016) 632–639, https://doi.org/10.1016/j.conbuildmat.2015.12.106.

[45] R. El-Hacha, Prestressing Concrete Structures with FRP Tendons (ACI 440.4R-04), 2005, https://doi.org/10.1061/40753(171)160.

[46] X. Wang, J. Shi, J. Liu, L. Yang, Z. Wu, Creep behavior of basalt fiber reinforced polymer tendons for prestressing application, Mater. Des. 59 (2014) 558–564, https://doi.org/10.1016/j.matdes.2014.03.009.

[47] W. Brameshuber, M. Hinzen, A. Dubey, A. Peled, B. Mobasher, A. Bentur, C. Aldea, F. Silva, J. Hegger, T. Gries, J. Wastiels, K. Malaga, C. Papanicolaou, L. Taerwe, M. Curbach, V. Mechtcherine, A. Naaman, J. Orlowsky, H. Patrice, F. Jesse, Recommendation of RILEM TC 232-TDT: Test methods and design of textile

[48] British Standards Institution (2011) BS EN 1170-5:1998: Precast concrete products. Test method for glass-fibre reinforced cement: Measuring bending strength, "complete bending test" method, British Standards Institution, London, 1998, https://doi.org/10.3403/01302372U.

[49] ASTM C 1018-97, Standard test method for flexural toughness and first-crack strength of fiber-reinforced concrete (using beam with third-point loading), American Society for Testing Materials, (2006), www.astm.org.

[50] R. Gilbert, N. Mickleborough, G. Ranzi, Design of Prestressed Concrete to Eurocode 2, 2017, https://doi.org/10.1201/9781315389523.

[51] N. Williams Portal, I. Fernandez Perez, L. Nyholm Thrane, K. Lundgren, Pull-out of textile reinforcement in concrete, Constr. Build. Mater. 71 (2014) 63–71, https://doi.org/10.1016/j.conbuildmat.2014.08.014.

[52] J. Hartig, F. Jesse, U. Häußler-Combe, Influence of different mechanisms on the constitutive behaviour of textile reinforced concrete, 2009.

[53] M. El Kadi, T. Tysmans, S. Verbruggen, J. Vervloet, M. De Munck, J. Wastiels, D. Van Hemelrijck, A layered-wise, composite modelling approach for fibre textile reinforced cementitious composites, Cem. Concr. Compos. 94 (2018) 107–115, https://doi.org/10.1016/j.cemconcomp.2018.08.015.

[54] L. Nahum, A. Peled, E. Gal, The flexural performance of structural concrete beams reinforced with carbon textile fabrics, Compos. Struct. 239 (2020), 111917, https://doi.org/10.1016/j.compstruct.2020.111917.

[55] D.H. Murcia, B. Çomak, E. Soliman, M.M. Reda Taha, Flexural Behavior of a Novel Textile-Reinforced Polymer Concrete, Polymers 14(1) (2022) 176, https://doi.org/10.3390/polym14010176.

[56] K. Orosz, T. Blanksvärd, B. Täljsten, G. Fischer, From Material Level to Structural Use of Mineral-Based Composites—An Overview, Adv. Civil Eng. 2010 (2010), 985843.

[57] S. Yin, S. Xu, H. Li, Improved mechanical properties of textile reinforced concrete thin plate, Journal of Wuhan University of Technology-Mater, Sci. Ed. 28 (1) (2013) 92–98, https://doi.org/10.1007/s11595-013-0647-z.

[58] U. Dilthey, Application of polymers in textile reinforced concrete - From the interface to construction elements, 2006, pp. 55-64, https://doi.org/10.1617/2351500087.006.

[59] J. Bielak, Y. Li, J. Hegger, R. Chudoba, Characterization Procedure for Bond, Anchorage and Strain-Hardening Behavior of Textile-Reinforced Cementitious Composites, Proceedings 2(8) (2018) 395, https://doi.org/10.3390/ICEM18-05224.

[60] D. Ngo, H.-C. Nguyen, Experimental and numerical investigations on flexural behaviour of prestressed textile reinforced concrete slabs, Civil Eng. J. 7 (2021) 1084–1097, https://doi.org/10.28991/cej-2021-03091712.

reinforced concrete, Mater. Struct. (2016), https://doi.org/10.1617/s11527-016-0839-z.